

Structure-Preserving Galerkin POD-DEIM Reduced-Order Modeling of Hamiltonian Systems

Zhu Wang ^{*}

Abstract

A structure preserving proper orthogonal decomposition reduce-order modeling approach has been developed in [1] for the Hamiltonian system, which uses the traditional framework of Galerkin projection-based model reduction but modifies the reduced order model so that the appropriate Hamiltonian structure is preserved. However, its computational complexity for online simulations is still high if the Hamiltonian involves non-polynomial nonlinearities. In this paper, we apply the discrete empirical interpolation method to improve the online efficiency of the structure-preserving reduced order simulations. Since the reduced basis truncation can degrade the Hamiltonian approximation, we propose to use the basis obtained from shifted snapshots. A nonlinear wave equation is used as a test bed and the numerical results illustrate the efficacy of the proposed method.

Keywords. Proper orthogonal decomposition; Discrete empirical interpolation method; model reduction; Hamiltonian systems; structure-preserving algorithms.

AMS subject classifications. 37M25, 65M99, 65P10, 93A15

1 Introduction

Hamiltonian systems have broad applications in engineering and scientific research. In real-world problems, using numerical methods to simulate such systems often leads to long-time integrations of large-scale discrete systems. Because the numerical error accumulates during simulations, preserving intrinsic properties of the systems has been a key criterion for developing stable numerical schemes. So far, geometric integrator or structure-preserving algorithms have been introduced to exactly preserve structural properties of Hamiltonian systems. For instance, symplectic algorithms proposed in [2, 3] has achieved a remarkable success in dealing with Hamiltonian ordinary differential equations (ODEs). They have been extended to Hamiltonian partial differential equations (PDEs) and preserve the multi-symplectic conservation law [4, 5]. In recent years, there has been an increasing emphasis on constructing numerical methods to preserve

^{*}Corresponding author. Department of Mathematics, University of South Carolina, Columbia, SC 29208. Email: wangzhu@math.sc.edu.

certain invariant quantities such as the total energy of continuous dynamical systems. Several discrete gradient methods have been proposed in the literature [6, 7, 8, 9, 10].

To accelerate the long-time, large-scale numerical simulations of the Hamiltonian systems, reduced-order modeling has been considered. One such model reduction technique is the proper orthogonal decomposition (POD) method, which has been successfully applied to many time-dependent, nonlinear PDEs ([11, 12, 13, 14, 15, 16, 17, 18, 19]). The POD method extracts orthogonal basis vectors from snapshot data, and use them to span the trial space. Based on different choices of test space, either Galerkin or Petrov-Galerkin projection can be used to build a low-dimensional dynamical system, which is the so-called reduced order model (ROM). However, they would destroy the Hamiltonian structure. This issue has been recently recognized and structure-preserving ROMs (SP-ROMs) have been developed to resolve it. For instance, structure-preserving Petrov-Galerkin reduced models were introduced in [20, 21] for port-Hamiltonian systems, in which the POD-based and \mathcal{H}_2 -based projection subspaces are considered. A proper symplectic decomposition approach using the symplectic Galerkin projection was proposed in [22] for Hamiltonian PDEs with a symplectic structure. A structure-preserving POD-ROM was introduced in [1], where the Galerkin projection-based ROM was modified so that appropriate Hamiltonian structure can be well kept. The approach has been applied to nonlinear Schrödinger equation and shallow water equations in [23, 24]. Although the SP-ROMs have a low dimension, when non-polynomial nonlinearities appear, their computational costs still depend on the number of spatial degrees of freedom in the full-order model. Thus, hyper-reduction method such as the discrete empirical interpolation method (DEIM) [25] has been employed as a remedy. It was combined with the Kronecker product in [26] to effectively reduce the complexity for evaluating the variable skew-symmetric coefficient matrix. In [21, 23], two different ways for applying DEIM to the gradient of Hamiltonian functions were proposed, respectively. It is worth mentioning that other types of model reduction techniques such as reduced basis method have been introduced for Hamiltonian systems as well [27, 28, 29, 29, 30]. There are ROMs investigated for preserving different geometric properties such as the Lagrangian structures in [31, 32].

In this paper, we use the framework of the SP-ROM developed in [1] and extend it to the case in which the gradient of Hamiltonian involves non-polynomial nonlinearities. A structure-preserving POD-DEIM ROM is then proposed that possesses the appropriate Hamiltonian structure while reducing the online simulation cost. Due to the basis truncation, there may exist discrepancies in the approximation to the Hamiltonian function between the new ROM and the full-order model. Therefore, we propose to use the POD basis and DEIM basis from shifted snapshots to improve the Hamiltonian approximation.

The rest of this paper is organized as follows. In Section 2, we introduce the SP-ROMs for Hamiltonian systems including the SP-POD and SP-DEIM models; The SP-ROMs are numerically investigated in Section 3; A few concluding remarks are drawn in the last section.

2 Structure-Preserving Galerkin ROMs

Consider a general Hamiltonian PDE system

$$\dot{\mathbf{u}} = \mathcal{D} \frac{\delta \mathcal{H}}{\delta \mathbf{u}}, \quad (2.1)$$

where \mathcal{D} is a differential operator and $\mathcal{H}(\mathbf{u})$ is the Hamiltonian, which often corresponds to the total energy of the system. When \mathcal{D} is a skew-adjoint operator with respect to the L_2 inner product, the PDE keeps $\mathcal{H}(\mathbf{u})$ invariant, which can be easily checked using the fact of $\int_{\Omega} \frac{\delta \mathcal{H}}{\delta \mathbf{u}} \mathcal{D} \frac{\delta \mathcal{H}}{\delta \mathbf{u}} dx = 0$. Note that when \mathcal{D} is a constant negative semi-definite (or definite) operator with respect to the L_2 inner product, the system becomes dissipative and $\mathcal{H}(\mathbf{u})$, usually referred to a Lyapunov function, would be non-increasing. In this paper, we shall focus on the former case, although the extension to the latter is straightforward.

Since (2.1) preserves the Hamiltonian, numerical methods for the PDE is expected to keep the same property at a discrete level. This has become a basic rule of thumb when designing a robust numerical scheme for the Hamiltonian PDE, especially for the purpose of long term simulations. Therefore, methods such as geometric integrators [2, 3, 4, 5] or structure-preserving algorithms [8, 33, 34, 9, 35, 10] have been developed to preserve such structural properties. On the other hand, for large-scale numerical simulations, in order to reduce the computational complexity, structure-preserving reduced order modeling has been introduced. Next, we first briefly review the structure-preserving approach proposed in [1], which modifies the standard Galerkin projection-based POD reduced order models for the Hamiltonian PDE, and then extend this approach to general nonlinear cases using DEIM and data-driven closure approaches.

2.1 The structure-preserving POD-ROM

A spatial discretization of (2.1) yields a finite n -dimensional Hamiltonian ODE system of the form (e.g. see [9]):

$$\dot{\mathbf{u}} = \mathbf{D} \nabla_{\mathbf{u}} H(\mathbf{u}) \quad (2.2)$$

with the initial condition $\mathbf{u}(t_0) = \mathbf{u}_0$ and appropriate boundary conditions. Note that we slightly abuse the notation here: \mathbf{u} is used again to denote the discrete state variable in \mathbb{R}^n . The coefficient matrix \mathbf{D} on the right-hand-side of (2.2) is skew-symmetric, whose size is n by n . We use the finite difference method in our numerical experiments, in which the dimension of the discrete variable, n , frequently equals to the number of grid points. $H : \mathbb{R}^n \rightarrow \mathbb{R}$ such that $H \Delta x$ provides a consistent approximation to the Hamiltonian $\mathcal{H}(\mathbf{u})$ associated to (2.1).

Given the $n \times r$ reduced basis matrix Φ , the state variable \mathbf{u} can be approximated by $\mathbf{u}_r(t) = \Phi \mathbf{a}(t)$, where $\mathbf{a}(t)$ is the unknown, r -dimensional coefficient vector. The reduced basis vectors can be determined at an offline stage by different model reduction techniques such as the reduced basis methods, proper orthogonal decomposition (POD), dynamical mode decomposition, etc. Here, we choose the POD because it is relatively easy to use and has been applied to many practical

engineering problems. A standard Galerkin projection-based reduced order model (G-ROM) reads:

$$\dot{\mathbf{a}} = \Phi^\top \mathbf{D} \nabla_{\mathbf{u}} H(\Phi \mathbf{a}). \quad (2.3)$$

It provides a low-dimensional surrogate to (2.2) since one only needs to solve for $\mathbf{a}(t)$ at the online stage and \mathbf{u}_r can be computed from the definition if needed. However, this model does not preserve the Hamiltonian function. It can be seen by checking the time derivate of $H_r(t) \equiv H(\Phi \mathbf{a}(t))$ as follows.

$$\begin{aligned} \frac{d}{dt} H(\Phi \mathbf{a}) &= [\nabla_{\mathbf{a}} H(\Phi \mathbf{a})]^\top \dot{\mathbf{a}} \\ &= [\Phi^\top \nabla_{\mathbf{u}} H(\Phi \mathbf{a})]^\top \Phi^\top \mathbf{D} \nabla_{\mathbf{u}} H(\Phi \mathbf{a}) \\ &= \nabla_{\mathbf{u}} H(\Phi \mathbf{a})^\top \Phi \Phi^\top \mathbf{D} \nabla_{\mathbf{u}} H(\Phi \mathbf{a}), \end{aligned}$$

where we use the fact that $\nabla_{\mathbf{a}} H(\Phi \mathbf{a}) = \Phi^\top \nabla_{\mathbf{u}} H(\Phi \mathbf{a})$. Since Φ is composed of r left singular vectors of the snapshot matrix, $\Phi \Phi^\top \mathbf{D}$ loses the skew-symmetry property of \mathbf{D} and the time derivative of $H(\Phi \mathbf{a})$ is not ensured to be zero.

The structure-preserving POD (SP-POD) reduced order model developed in [1] modifies the approach such that the Hamiltonian function is well preserved, which has the following form:

$$\dot{\mathbf{a}} = \mathbf{D}_r \nabla_{\mathbf{a}} H(\Phi \mathbf{a}), \quad (2.4)$$

where $\mathbf{D}_r = \Phi^\top \mathbf{D} \Phi$. For this reduced-order dynamical system, the time derivative of $H_r(t)$ is

$$\begin{aligned} \frac{d}{dt} H(\Phi \mathbf{a}) &= [\nabla_{\mathbf{a}} H(\Phi \mathbf{a})]^\top \dot{\mathbf{a}} \\ &= [\nabla_{\mathbf{a}} H(\Phi \mathbf{a})]^\top \mathbf{D}_r \nabla_{\mathbf{a}} H(\Phi \mathbf{a}) \\ &= 0, \quad \text{as } \mathbf{D}_r \text{ is skew-symmetric.} \end{aligned}$$

Hence, this reduced order model possesses an invariant $H_r(t)$. Using a structure preserving time stepping, the discrete Hamiltonian $H_r \Delta x$ can be well preserved during long-term simulations.

2.2 The structure-preserving DEIM-ROM

Although the reduced order model (2.4) has a low dimension, its computational cost could still depend on the number of spatial degrees of freedom if $\mathbf{D} \equiv \mathbf{D}(\mathbf{u})$ depends nonlinearly on \mathbf{u} or $\nabla_{\mathbf{u}} H(\mathbf{u})$ includes non-polynomial nonlinearities. In either case, online simulations involve certain calculations to be performed at all the grid points. To overcome this issue, hyper-reduction methods such as DEIM have to be used. For instance, DEIM is combined with the Kronecker product in [26] to effectively reduce the complexity for evaluating $\mathbf{D}(\Phi \mathbf{a})$. We shall focus on the latter case in this paper. For completeness of presentation, we next first present the DEIM algorithm, review existing DEIM hamiltonian approximations, and then introduce a new approach.

In general, the DEIM employs the following ansatz on a nonlinear function $f(\mathbf{u}(t))$:

$$f(\mathbf{u}(t)) = \sum_{j=1}^s \psi_j c_j(t), \quad (2.5)$$

where ψ_j is the j -th nonlinear POD basis vectors generated from the nonlinear snapshots

$$[f(\mathbf{u}(t_1)), f(\mathbf{u}(t_2)), \dots, f(\mathbf{u}(t_m))].$$

Define the DEIM basis matrix $\Psi = [\psi_1, \dots, \psi_s] \in \mathbb{R}^{n \times s}$, the DEIM, as shown in Algorithm 1, selects a set of interpolation points $\varphi := [\varphi_1, \dots, \varphi_s]^\top \in \mathbb{R}^s$ in a greedy manner, in which e_{φ_i} be the φ_i -th column in the identity matrix.

Algorithm 1: DEIM

```

input :  $\{\psi_\ell\}_{\ell=1}^s \subset \mathbb{R}^s$  linear independent
output:  $\varphi = [\varphi_1, \dots, \varphi_s]^\top \in \mathbb{R}^s$ 
 $[\|\rho\|, \varphi_1] = \max\{|\psi_1|\};$ 
 $\Psi = [\psi_1], \mathbf{P} = [e_{\varphi_1}], \varphi = [\varphi_1];$ 
for  $\ell = 2$  to  $s$  do
   $\left| \begin{array}{l} \text{Solve } (\mathbf{P}^\top \Psi) \mathbf{c} = \mathbf{P}^\top \psi_\ell \text{ for } \mathbf{c} ; \\ \mathbf{r} = \psi_\ell - \Psi \mathbf{c}; \\ [\|\rho\|, \varphi_\ell] = \max\{|\mathbf{r}|\}; \\ \Psi \leftarrow [\Psi \quad \psi_\ell], \mathbf{P} \leftarrow [\mathbf{P} \quad e_{\varphi_\ell}], \varphi \leftarrow \begin{bmatrix} \varphi \\ \varphi_\ell \end{bmatrix}; \end{array} \right.$ 

```

The DEIM approximation of the nonlinear function is given by

$$f(\mathbf{u}) \approx \Psi(\mathbf{P}^\top \Psi)^{-1} \mathbf{P}^\top f(\mathbf{u}), \quad (2.6)$$

where $\mathbf{P} = [e_{\varphi_1}, \dots, e_{\varphi_s}] \in \mathbb{R}^{n \times s}$ is the matrix for selecting the corresponding s indices $\varphi_1, \dots, \varphi_s$. For a detailed description of the method, the read is referred to [13].

When the discrete Hamiltonian contains non-polynomial nonlinear functions of \mathbf{u} , the gradient $\nabla_{\mathbf{u}} H(\mathbf{u})$ usually includes non-polynomial nonlinearities as well. It makes the computational complexity depending on n , the number of degrees of freedom of the full-order model. To reduce the online simulation cost, a DEIM hamiltonian was proposed in [21]. It splits $H(\mathbf{u})$ into two parts:

$$H(\mathbf{u}) = \frac{1}{2} \mathbf{u}^\top \mathbf{Q} \mathbf{u} + h(\mathbf{u}). \quad (2.7)$$

The first part is quadratic in \mathbf{u} , where \mathbf{Q} is an $n \times n$ positive definite, constant matrix, and the second one is the remainder. When computing the gradient of $H(\mathbf{u})$, the first part provides its linear component, while the second part represents the nonlinearity of $\nabla_{\mathbf{u}} H(\mathbf{u})$. It is natural to approximate $\nabla_{\mathbf{u}} h(\mathbf{u})$ by a DEIM interpolation: $\nabla_{\mathbf{u}} h(\mathbf{u}(t)) \approx \Psi(\mathbf{P}^\top \Psi)^{-1} \mathbf{P}^\top \nabla_{\mathbf{u}} h(\mathbf{u}(t))$. Denote the DEIM projection by $\mathbb{P} = \Psi(\mathbf{P}^\top \Psi)^{-1} \mathbf{P}^\top$, one can define the DEIM Hamiltonian by

$$\widehat{H}(\mathbf{u}) = \frac{1}{2} \mathbf{u}^\top \mathbf{Q} \mathbf{u} + h(\mathbb{P}^\top \mathbf{u}),$$

whose gradient is

$$\nabla_{\mathbf{u}} \widehat{H}(\mathbf{u}) = \mathbf{Q} \mathbf{u} + \mathbb{P} \nabla_{\mathbf{u}} h(\mathbb{P}^\top \mathbf{u}).$$

Then if in reduced Hamiltonian $\widehat{H}_r(t) \equiv \widehat{H}(\Phi\mathbf{a}(t))$, it can be shown that $\widehat{H}_r(t)$ is invariant. However, the DEIM projection \mathbb{P} is derived from snapshots of $\nabla_{\mathbf{u}}h(\mathbf{u})$, and \mathbf{u} is approximated by $\mathbb{P}^\top \mathbf{u}$, which introduces approximation errors.

In [23], nonlinear functions in $\nabla_{\mathbf{u}}H(\mathbf{u})$ are directly approximated by the DEIM interpolation. Suppose a nonlinear component in the gradient of the reduced order model is $\Phi^\top \nabla_{\mathbf{u}}h(\Phi\mathbf{a})$, then the DEIM approximation reads

$$\Phi^\top \nabla_{\mathbf{u}}h(\Phi\mathbf{a}) \approx \Phi^\top \mathbb{P} \nabla_{\mathbf{u}}h(\Phi\mathbf{a}).$$

This way avoids approximating \mathbf{u}_r by $\mathbb{P}^\top \mathbf{u}_r$ in the reduced order simulation, but there does not exist an explicit expression of the discrete Hamiltonian. As a result, this approach cannot preserve the discrete energy exactly.

Therefore, we propose a new way to deal with the nonlinearity in the gradient of $H(\mathbf{u})$ so that the computational complexity of nonlinear function evaluations while keeping the Hamiltonian invariant at the discrete level. The key idea is to apply DEIM to the Hamiltonian function, not to its gradient. To this end, we first recognize a discrete Hamiltonian function can usually be formulated as follows:

$$H(\mathbf{u}) = \frac{1}{2} \mathbf{u}^\top \mathbf{Q} \mathbf{u} + \mathbf{c}^\top \mathbf{G}(\mathbf{u}),$$

where \mathbf{G} is a nonlinear vector-valued function of \mathbf{u} , and $\mathbf{c}^\top \mathbf{G}(\mathbf{u})$ represents the non-polynomial nonlinearity. After collecting snapshots of $\mathbf{G}(\mathbf{u})$, $[\mathbf{G}(\mathbf{u}(t_0), \dots, \mathbf{G}(\mathbf{u}(t_m))]$, we apply POD to obtain DEIM basis Ψ . Suppose an interpolation point index set $\{p_1, \dots, p_s\}$ and matrix $\mathbf{P} = [e_{p_1}, \dots, e_{p_s}] \in \mathbb{R}^{n \times s}$ are output from Algorithm 1, the DEIM interpolation of $\mathbf{G}(\mathbf{u})$ reads:

$$\mathbf{G}(\mathbf{u}) \approx \mathbb{P} \mathbf{G}(\mathbf{u}) = \Psi(\mathbf{P}^\top \Psi)^{-1} \mathbf{P}^\top \mathbf{G}(\mathbf{u}).$$

Then the reduced Hamiltonian can be defined as

$$H_r(t) \equiv H(\Phi\mathbf{a}) = \frac{1}{2} \mathbf{a}^\top \mathbf{Q}_r \mathbf{a} + \mathbf{c}^\top \mathbb{P} \mathbf{G}(\Phi\mathbf{a}), \quad (2.8)$$

with $\mathbf{Q}_r = \Phi^\top \mathbf{Q} \Phi$ and the associated gradient can be expressed as

$$\nabla_{\mathbf{a}} H_r(\mathbf{a}) = \mathbf{Q}_r \mathbf{a} + \Phi^\top \mathbf{J}_{\mathbf{G}}(\Phi\mathbf{a}) \mathbb{P}^\top \mathbf{c}, \quad (2.9)$$

where $\mathbf{J}_{\mathbf{G}}(\cdot)$ is the Jacobian matrix of $\mathbf{G}(\mathbf{u})$. Plugging (2.9) into (2.4), we have a structure-preserving DEIM (SP-DEIM) model:

$$\begin{aligned} \dot{\mathbf{a}} &= \mathbf{D}_r \nabla_{\mathbf{a}} H(\Phi\mathbf{a}) \\ &= \mathbf{D}_r [\mathbf{Q}_r \mathbf{a} + \Phi^\top \mathbf{J}_{\mathbf{G}}(\Phi\mathbf{a}) \mathbb{P}^\top \mathbf{c}]. \end{aligned} \quad (2.10)$$

Using the same argument as (2.5), we can easily show the discrete Hamiltonian $H_r(t)$ is invariant.

2.3 Improvement of the Hamiltonian approximation

Although a small amount of POD basis functions captures most of the snapshot information, the basis truncation would result in a loss of information. It further leads to a discrepancy in the Hamiltonian function approximation between the ROM and the FOM. Since the proposed structure-preserving ROMs are able to keep a constant Hamiltonian in the reduced-order simulation, such a discrepancy stays unchanged from the beginning of the simulations. To overcome this issue, we need to adjust the initial value of the discrete Hamiltonian. Therefore, we follow one approach developed in [1] that uses the POD basis generated from shifted snapshots.

Instead of considering the snapshots of state variables, $[\mathbf{u}(t_1), \dots, \mathbf{u}(t_M)]$, we use a shifted snapshot set

$$[\mathbf{u}(t_1) - \mathbf{u}_0, \dots, \mathbf{u}(t_M) - \mathbf{u}_0] \quad (2.11)$$

and obtain the POD basis Φ . The related reduced approximation becomes

$$\mathbf{u}_r(t) = \Phi \mathbf{a}(t) + \mathbf{u}_0. \quad (2.12)$$

Accordingly, we generate DEIM basis Ψ from a shifted nonlinear snapshot set

$$[\mathbf{G}(\mathbf{u}(t_1)) - \mathbf{G}(\mathbf{u}_0), \dots, \mathbf{G}(\mathbf{u}(t_M)) - \mathbf{G}(\mathbf{u}_0)]. \quad (2.13)$$

The related DEIM approximation becomes $\mathbb{P}(\mathbf{G}(\mathbf{u}) - \mathbf{G}(\mathbf{u}_0)) + \mathbf{G}(\mathbf{u}_0)$, where \mathbb{P} is the DEIM projection. The reduced Hamiltonian is

$$H_r(t) = \frac{1}{2}(\mathbf{u}_0^\top + \mathbf{a}^\top \Phi^\top) \mathbf{Q}(\Phi \mathbf{a} + \mathbf{u}_0) + \mathbf{c}^\top [\mathbb{P} \mathbf{G}(\Phi \mathbf{a} + \mathbf{u}_0) + (\mathbb{I} - \mathbb{P}) \mathbf{G}(\mathbf{u}_0)], \quad (2.14)$$

which matches $H(\mathbf{u}_0)$ at the initial time.

Substituting (2.14) into (2.4), we have

$$\begin{aligned} \dot{\mathbf{a}} &= \mathbf{D}_r \nabla_{\mathbf{a}} H(\Phi \mathbf{a} + \mathbf{u}_0) \\ &= \mathbf{D}_r [\mathbf{Q}_r \mathbf{a} + \Phi^\top \mathbf{Q} \mathbf{u}_0 + \Phi^\top \mathbf{J}_G(\Phi \mathbf{a} + \mathbf{u}_0) \mathbb{P}^\top \mathbf{c}], \end{aligned} \quad (2.15)$$

together with the initial condition $\mathbf{a}(t_0) = \mathbf{0}$. Since \mathbf{D}_r is skew symmetric, the model preserves the structural property and the reduced Hamiltonian would keep the same value as $H(\mathbf{u}_0)$ during the reduced order simulations.

3 Numerical experiments

In this section, we use a nonlinear wave equation as an example of Hamiltonian PDEs to investigate the numerical performance of the structure-preserving ROMs.

Consider the one-dimensional case with a constant moving speed c and a nonlinear forcing term $g(u)$,

$$u_{tt} = c^2 u_{xx} - g(u), \quad 0 \leq x \leq l.$$

The equation can be written in the Hamiltonian formulation

$$\begin{bmatrix} \dot{u} \\ \dot{v} \end{bmatrix} = \begin{bmatrix} 0 & 1 \\ -1 & 0 \end{bmatrix} \begin{bmatrix} \frac{\delta \mathcal{H}}{\delta u} \\ \frac{\delta \mathcal{H}}{\delta v} \end{bmatrix},$$

which has a symplectic structure. The PDE system has a constant the Hamiltonian that is also the total energy:

$$\mathcal{H}(t) = \int_0^l \left[\frac{1}{2} v^2 + \frac{c^2}{2} u_x^2 + G(u) \right] dx,$$

where $G'(u) = g(u)$, $\frac{\delta \mathcal{H}}{\delta u} = -c^2 u_{xx} + g(u)$ and $\frac{\delta \mathcal{H}}{\delta v} = v$. After a spatial discretization using finite difference method with n uniformly distributed grid points with mesh size Δx , (3) is rewritten into

$$\begin{bmatrix} \dot{\mathbf{u}} \\ \dot{\mathbf{v}} \end{bmatrix} = \begin{bmatrix} 0 & \mathbf{I}_n \\ -\mathbf{I}_n & 0 \end{bmatrix} \begin{bmatrix} -\mathbf{A}\mathbf{u} + \mathbf{G}'(\mathbf{u}) \\ \mathbf{v} \end{bmatrix}, \quad (3.16)$$

where \mathbf{A} is a discrete, scaled, one-dimensional second order differential operator, $\mathbf{G}(\mathbf{u})$ denotes the discretization of the nonlinear function $G(u)$ and the coefficient matrix is symplectic, also skew-symmetric. The discrete Hamiltonian is $H\Delta x$ with

$$H(t) = \frac{1}{2} \mathbf{v}^\top \mathbf{v} - \frac{1}{2} \mathbf{u}^\top \mathbf{A} \mathbf{u} + \mathbf{c}^\top \mathbf{G}(\mathbf{u}),$$

in which \mathbf{c} is the all-ones vector.

The problem has been tested by a proper symplectic decomposition method in [22]. The linear case, when $g(u) = 0$, has been investigated in [1]. Here we focus on the nonlinear case $g(u) = \sin(u)$ with $G(u) = 1 - \cos(u)$, $[\mathbf{G}(\mathbf{u})]_i = 1 - \cos(u_i)$ and $[\mathbf{g}(\mathbf{u})]_i = \sin(u_i)$ for $i = 0, \dots, n-1$. In particular, we choose $c = 0.1$, $x \in [0, 1]$, $t \in [0, 50]$, and periodic boundary conditions. The initial condition satisfies $u(0) = f(s(x))$ and $\dot{u}(0) = 0$, where $f(s)$ is a cubic spline function defined by

$$f(s) = \begin{cases} 1 - \frac{3}{2}s^2 + \frac{3}{4}s^3 & \text{if } 0 \leq s \leq 1, \\ \frac{1}{4}(2-s)^3 & \text{if } 1 < s \leq 2, \\ 0 & \text{if } s > 2, \end{cases}$$

and $s(x) = 10|x - \frac{1}{2}|$.

In a full-order simulation, the spatial domain is partitioned into $n = 500$ equal subintervals, thus the mesh size $\Delta x = 2 \times 10^{-3}$. We use the symplectic midpoint method for the time integration with a time step $\Delta t = 0.01$. A three-point stencil finite difference method is taken for the spatial discretization of the 1D Laplacian operator. The full order solution at time t_{k+1} , \mathbf{u}_h^{k+1} and \mathbf{v}_h^{k+1} , satisfies

$$\begin{bmatrix} \frac{\mathbf{u}_h^{k+1} - \mathbf{u}_h^k}{\Delta t} \\ \frac{\mathbf{v}_h^{k+1} - \mathbf{v}_h^k}{\Delta t} \end{bmatrix} = \begin{bmatrix} 0 & \mathbf{I}_n \\ -\mathbf{I}_n & 0 \end{bmatrix} \begin{bmatrix} -\mathbf{A} \frac{\mathbf{u}_h^{k+1} + \mathbf{u}_h^k}{2} + \mathbf{g} \left(\frac{\mathbf{u}_h^{k+1} + \mathbf{u}_h^k}{2} \right) \\ \frac{\mathbf{v}_h^{k+1} + \mathbf{v}_h^k}{2} \end{bmatrix},$$

where

$$\mathbf{A} = \frac{c^2}{\Delta x^2} \begin{pmatrix} -2 & 1 & 0 & 0 & \cdots & 1 \\ 1 & -2 & 1 & 0 & \cdots & 0 \\ \ddots & \ddots & \ddots & & & \\ 0 & \cdots & 0 & 1 & -2 & 1 \\ 1 & \cdots & 0 & 0 & 1 & -2 \end{pmatrix},$$

the initial data \mathbf{u}_h^0 has the i -th component equals $h(s(x_i))$ for $1 \leq i \leq n$ and $\mathbf{v}_h^0 = \mathbf{0}$. The system is nonlinear that is solved by the Picard iteration.

It takes 52.8 seconds to finish the simulation. The time evolution of numerical solutions \mathbf{u}_h and \mathbf{v}_h and the discrete energy $H\Delta x$ of the full-order results are plotted in Figure 1. It is seen that the discrete energy is around 1.258×10^{-1} . It is not exactly preserved due to the use of midpoint scheme. Since the exact solution is unknown, in what follows, this full-order simulation

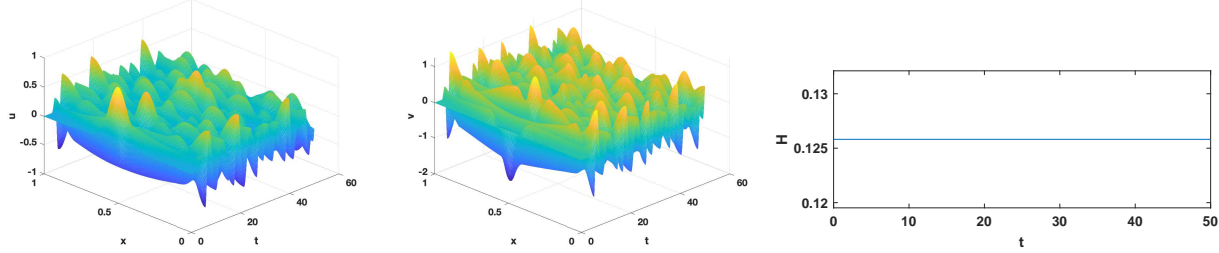


Figure 1: Full-order model simulation: time evolution of \mathbf{u}_h (left), time evolution of \mathbf{v}_h (middle), and energy evolution $H\Delta x$ (right).

results will be served as benchmark solution for ROMs.

Next, we investigate the numerical performance of three types of ROMs: i) the POD-G model; ii) the SP-POD ROMs; iii) the SP-DEIM ROMs. The criteria we shall use include: the maximum approximation error over the entire spatial-temporal domain,

$$\mathcal{E}_\infty = \max_{k \geq 0} \max_{0 \leq i \leq n} \sqrt{[(\mathbf{u}_h^k)_i - (\mathbf{u}_r^k)_i]^2 + [(\mathbf{v}_h^k)_i - (\mathbf{v}_r^k)_i]^2},$$

the energy value in the reduced-order simulation $H_r\Delta x$, and the CPU time t_{cpu} for online simulations.

3.1 Standard POD-G ROM.

Snapshots are collected from the full-order simulation every 50 time steps. Using the singular value decomposition, we find the r -dimensional POD basis Φ_u and Φ_v for functions u and v , respectively. The standard POD-G ROM is generated by substituting the POD approximation $\mathbf{u}_r(t) = \Phi_u \mathbf{a}(t)$ and $\mathbf{v}_r(t) = \Phi_v \mathbf{b}(t)$ into (3.16) and applying the Galerkin projection, which can be written as:

$$\begin{bmatrix} \dot{\mathbf{a}} \\ \dot{\mathbf{b}} \end{bmatrix} = \begin{bmatrix} \Phi_u^\top \Phi_v \mathbf{b} \\ \Phi_v^\top \mathbf{A} \Phi_u \mathbf{a} - \Phi_v^\top \mathbf{g}(\Phi_u \mathbf{a}) \end{bmatrix}.$$

By using the same time integration method as the full order model, we have the POD basis coefficient at t_{k+1} , \mathbf{a}^{k+1} and \mathbf{b}^{k+1} , satisfying

$$\begin{bmatrix} \frac{\mathbf{a}^{k+1}-\mathbf{a}^k}{\Delta t} \\ \frac{\mathbf{b}^{k+1}-\mathbf{b}^k}{\Delta t} \end{bmatrix} = \begin{bmatrix} \Phi_u^\top \Phi_v \frac{\mathbf{b}^{k+1}+\mathbf{b}^k}{2} \\ \Phi_v^\top \mathbf{A} \Phi_u \frac{\mathbf{a}^{k+1}+\mathbf{a}^k}{2} - \Phi_v^\top \mathbf{g}(\Phi_u \frac{\mathbf{a}^{k+1}+\mathbf{a}^k}{2}) \end{bmatrix}$$

with the initial condition $\mathbf{a}^0 = \Phi_u^\top \mathbf{u}_0$ and $\mathbf{b}^0 = \Phi_v^\top \mathbf{v}_0$.

For $r = 10$ and 20 , the respective CPU times for online simulations are 0.765 seconds and 0.979 seconds. The associated maximum errors of the reduced approximations are $\mathcal{E}_\infty = 3.291 \times 10^{-2}$ and 8.288×10^{-3} , respectively. The time evolution of Hamiltonian approximation errors for both cases is shown in Figure 2. It is observed that the order of Hamiltonian approximation errors varies from $\mathcal{O}(10^{-5})$ when $r = 10$ to $\mathcal{O}(10^{-7})$ when $r = 20$. As r increases, the discrete Hamiltonian becomes more accurate, but it is not time invariant as the standard POD-G ROM is not structure preserving.

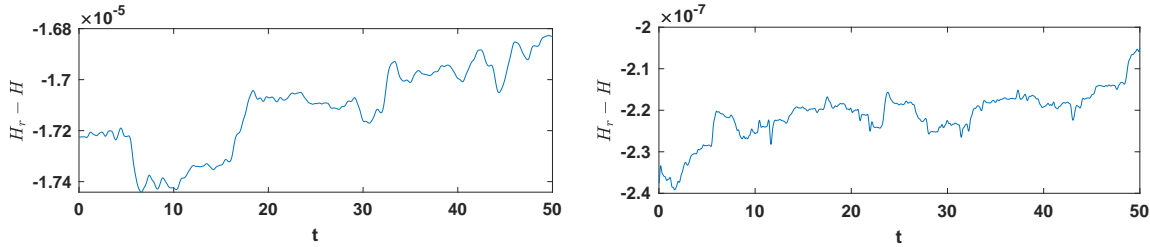


Figure 2: $H_r \Delta x - H \Delta x$ of the Standard POD-ROM: $r = 10$ (left) and $r = 20$ (right).

3.2 The SP-POD Models.

Next, we consider the structure-preserving ROMs introduced in Section 2. Two SP-POD ROMs are applied: the first one uses the standard POD basis, named SP-POD-1; the other uses the POD basis generated from shifted snapshots, named SP-POD-2.

SP-POD-1. This SP-ROM has the following form:

$$\begin{bmatrix} \dot{\mathbf{a}} \\ \dot{\mathbf{b}} \end{bmatrix} = \begin{bmatrix} 0 & \Phi_u^\top \Phi_v \\ -\Phi_v^\top \Phi_u & 0 \end{bmatrix} \begin{bmatrix} -\mathbf{A}_r \mathbf{a} + \Phi_u^\top \mathbf{g}(\Phi_u \mathbf{a}) \\ \mathbf{b} \end{bmatrix},$$

where $\mathbf{A}_r = \Phi_u^\top \mathbf{A} \Phi_u$. The coefficient matrix on the right-hand-side of the system is skew-symmetric, which has the same structure as that of the full-order model. Thus, we expect a constant discrete Hamiltonian in the reduced-order simulation. Using the symplectic midpoint scheme, the discrete system reads:

$$\begin{bmatrix} \frac{\mathbf{a}^{k+1}-\mathbf{a}^k}{\Delta t} \\ \frac{\mathbf{b}^{k+1}-\mathbf{b}^k}{\Delta t} \end{bmatrix} = \begin{bmatrix} 0 & \Phi_u^\top \Phi_v \\ -\Phi_v^\top \Phi_u & 0 \end{bmatrix} \begin{bmatrix} -\mathbf{A}_r \frac{\mathbf{a}^{k+1}+\mathbf{a}^k}{2} + \Phi_u^\top \mathbf{g}(\Phi_u \frac{\mathbf{a}^{k+1}+\mathbf{a}^k}{2}) \\ \frac{\mathbf{b}^{k+1}+\mathbf{b}^k}{2} \end{bmatrix} \quad (3.17)$$

with the initial condition $\mathbf{a}^0 = \Phi_u^\top \mathbf{u}_0$ and $\mathbf{b}^0 = \Phi_v^\top \mathbf{v}_0$.

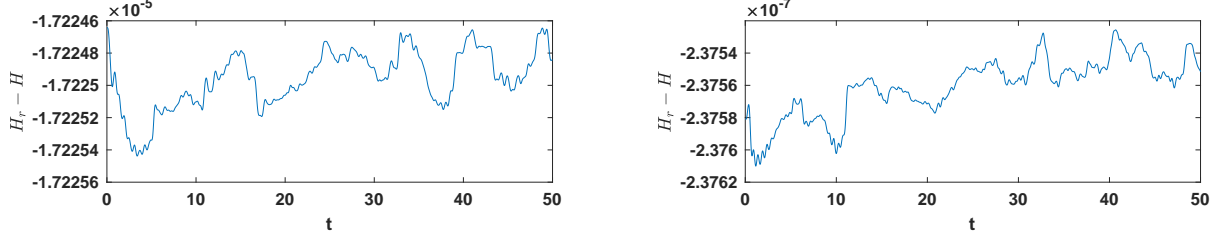


Figure 3: $H_r\Delta x - H\Delta x$ of the SP-POD-1: $r = 10$ (left) and $r = 20$ (right).

It takes 0.601 seconds and 0.786 seconds to complete the simulations of SP-POD-1 model with dimensions $r = 10$ and $r = 20$, respectively. The corresponding maximum errors of the reduced approximation is $\mathcal{E}_\infty = 3.291 \times 10^{-2}$ and 8.298×10^{-3} . Errors of the Hamiltonian approximations in both cases are presented in Figure 3. It is seen that $H_r\Delta x - H\Delta x$ possesses the same magnitude as that in the standard POD-G model of the same dimensions. This is because the POD truncation causes information loss, which results in the Hamiltonian approximation error. Therefore, we next correct the reduced Hamiltonian by using the POD basis from shifted snapshots.

SP-POD-2. This SP-ROM has the following form:

$$\begin{bmatrix} \dot{\mathbf{a}} \\ \dot{\mathbf{b}} \end{bmatrix} = \begin{bmatrix} 0 & \Phi_u^\top \Phi_v \\ -\Phi_v^\top \Phi_u & 0 \end{bmatrix} \begin{bmatrix} -\mathbf{A}_r \mathbf{a} - \Phi_u^\top \mathbf{A} \mathbf{u}_0 + \Phi_u^\top \mathbf{g}(\Phi_u \mathbf{a} + \mathbf{u}_0) \\ \mathbf{b} + \Phi_v^\top \mathbf{v}_0 \end{bmatrix}. \quad (3.18)$$

Using the same symplectic midpoint method, we have the discrete system as follows.

$$\begin{bmatrix} \frac{\mathbf{a}^{k+1} - \mathbf{a}^k}{\Delta t} \\ \frac{\mathbf{b}^{k+1} - \mathbf{b}^k}{\Delta t} \end{bmatrix} = \begin{bmatrix} 0 & \Phi_u^\top \Phi_v \\ -\Phi_v^\top \Phi_u & 0 \end{bmatrix} \begin{bmatrix} -\mathbf{A}_r \frac{\mathbf{a}^{k+1} + \mathbf{a}^k}{2} - \Phi_u^\top \mathbf{A} \mathbf{u}_0 + \Phi_u^\top \mathbf{g}(\Phi_u \frac{\mathbf{a}^{k+1} + \mathbf{a}^k}{2} + \mathbf{u}_0) \\ \frac{\mathbf{b}^{k+1} + \mathbf{b}^k}{2} + \Phi_v^\top \mathbf{v}_0 \end{bmatrix} \quad (3.19)$$

with the initial condition $\mathbf{a}^0 = \mathbf{0}$ and $\mathbf{b}^0 = \mathbf{0}$.

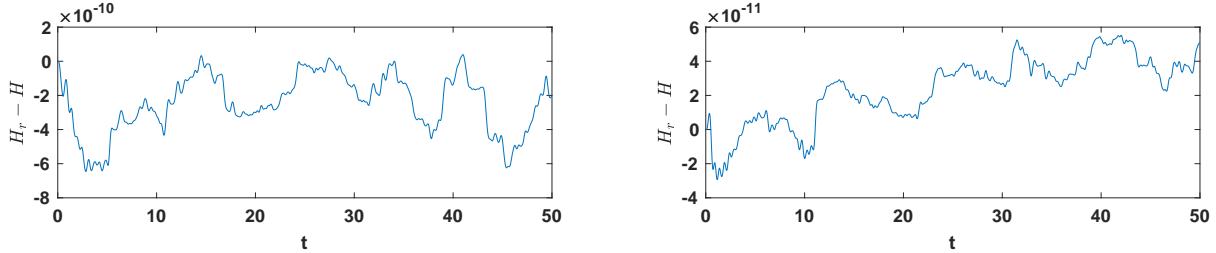


Figure 4: $H_r\Delta x - H\Delta x$ of the SP-POD-2: $r = 10$ (left) and $r = 20$ (right).

The CPU times of the simulations when $r = 10$ and 20 are 0.630 seconds and 0.805 seconds, respectively. The corresponding maximum errors are $\mathcal{E}_\infty = 3.711 \times 10^{-2}$ and 1.015×10^{-2} . Figure 4 displays the time history of the discrete Hamiltonian values during the simulations in both cases. Compared with those obtained from SP-POD-1 model, the Hamiltonian approximation errors of SP-POD-2 shrink to $\mathcal{O}(10^{-10})$ and $\mathcal{O}(10^{-11})$ in these two cases. This illustrates the advantage of using POD basis from shifted snapshots for improving the energy approximation.

3.3 The SP-DEIM Models

The SP-POD models still have the computational complexity dependent on the number of degrees of freedom in the full-order simulations due to the nonlinearity of $\mathbf{g}(\cdot)$. To reduce the computational cost, we next utilize the SP-DEIM ROMs. Two types of models are applied: the first one is named by SP-DEIM-1 that uses the standard POD and DEIM basis, the other one is named SP-DEIM-2 that uses the POD basis from shifted state snapshots and DEIM basis generated from the shifted nonlinear snapshots. In both models, we select the number of DEIM basis to be twice as many as that of POD basis.

SP-DEIM-1. This model has the following form:

$$\begin{bmatrix} \dot{\mathbf{a}} \\ \dot{\mathbf{b}} \end{bmatrix} = \begin{bmatrix} 0 & \Phi_u^\top \Phi_v \\ -\Phi_v^\top \Phi_u & 0 \end{bmatrix} \begin{bmatrix} -\mathbf{A}_r \mathbf{a} + \Phi_u^\top \mathbf{g}(\Phi_u \mathbf{a}) \mathbb{P}^\top C \\ \mathbf{b} \end{bmatrix}. \quad (3.20)$$

With the symplectic midpoint rule, we have

$$\begin{bmatrix} \frac{\mathbf{a}^{k+1} - \mathbf{a}^k}{\Delta t} \\ \frac{\mathbf{b}^{k+1} - \mathbf{b}^k}{\Delta t} \end{bmatrix} = \begin{bmatrix} 0 & \Phi_u^\top \Phi_v \\ -\Phi_v^\top \Phi_u & 0 \end{bmatrix} \left(\begin{bmatrix} -\mathbf{A}_r \frac{\mathbf{a}^{k+1} + \mathbf{a}^k}{2} + \Phi_u^\top \mathbf{g}(\Phi_u \frac{\mathbf{a}^{k+1} + \mathbf{a}^k}{2}) \mathbb{P}^\top C \\ \frac{\mathbf{b}^{k+1} + \mathbf{b}^k}{2} \end{bmatrix} \right) \quad (3.21)$$

with the initial condition $\mathbf{a}^0 = \Phi_u^\top \mathbf{u}_0$ and $\mathbf{b}^0 = \Phi_v^\top \mathbf{v}_0$.

For $r = 10$ and 20 , it respectively takes 0.141 seconds and 0.209 seconds to complete the simulations. Correspondingly, the maximum errors of the reduced-order simulation are $\mathcal{E}_\infty = 3.364 \times 10^{-2}$ and 8.473×10^{-3} . The errors of Hamiltonian function approximations in both cases are presented in Figure 5. Their magnitudes are close to those obtained by the SP-POD-1 model.

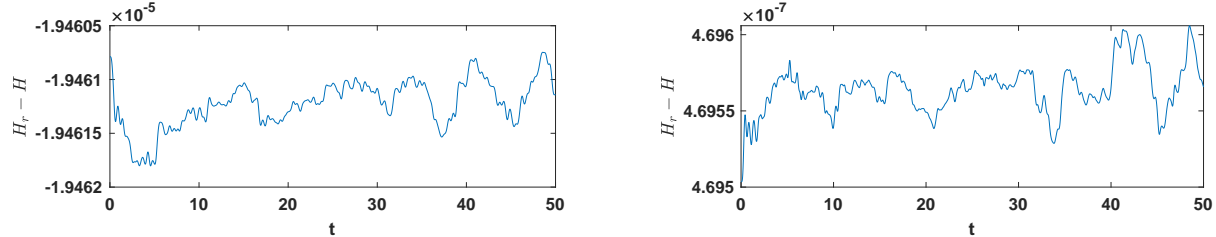


Figure 5: Time evolution of energy error $H_r \Delta x - H \Delta x$ in SP-DEIM-1: $r = 10$ (left) and $r = 20$ (right).

SP-DEIM-2. To improve the discrete Hamiltonian, we use the POD basis generated from shifted state snapshots and the DEIM basis from shifted nonlinear snapshots. The model has the following form:

$$\begin{bmatrix} \dot{\mathbf{a}} \\ \dot{\mathbf{b}} \end{bmatrix} = \begin{bmatrix} 0 & \Phi_u^\top \Phi_v \\ -\Phi_v^\top \Phi_u & 0 \end{bmatrix} \begin{bmatrix} -\mathbf{A}_r \mathbf{a} - \Phi_u^\top \mathbf{A} \mathbf{u}_0 + \Phi_u^\top \mathbf{g}(\Phi_u \mathbf{a} + \mathbf{u}_0) \mathbb{P}^\top C \\ \mathbf{b} + \Phi_v^\top \mathbf{v}_0 \end{bmatrix}. \quad (3.22)$$

After applying the symplectic midpoint rule, we have

$$\begin{bmatrix} \frac{\mathbf{a}^{k+1} - \mathbf{a}^k}{\Delta t} \\ \frac{\mathbf{b}^{k+1} - \mathbf{b}^k}{\Delta t} \end{bmatrix} = \begin{bmatrix} 0 & \Phi_u^\top \Phi_v \\ -\Phi_v^\top \Phi_u & 0 \end{bmatrix} \begin{bmatrix} -\mathbf{A}_r \frac{\mathbf{a}^{k+1} + \mathbf{a}^k}{2} - \Phi_u^\top \mathbf{A} \mathbf{u}_0 + \Phi_u^\top \mathbf{g}(\Phi_u \frac{\mathbf{a}^{k+1} + \mathbf{a}^k}{2} + \mathbf{u}_0) \mathbb{P}^\top \mathbf{C} \\ \frac{\mathbf{b}^{k+1} + \mathbf{b}^k}{2} + \Phi_v^\top \mathbf{v}_0 \end{bmatrix} \quad (3.23)$$

with the initial condition $\mathbf{a}^0 = \mathbf{0}$ and $\mathbf{b}^0 = \mathbf{0}$.

The CPU times for online simulations when $r = 10$ and 20 are 0.143 seconds and 0.210 seconds, respectively. The associated maximum errors are $\mathcal{E}_\infty = 3.490 \times 10^{-2}$ and 1.311×10^{-2} . The errors are bigger than those obtained from the SP-POD-2 model, which can be improved by increasing the number of DEIM basis and interpolation points. The Hamiltonian function approximation errors for both cases are presented in Figure 6, whose magnitude are close to those in the SP-POD-2 simulations. It illustrates the SP-DEIM-2 model is able to preserve the discrete Hamiltonian.

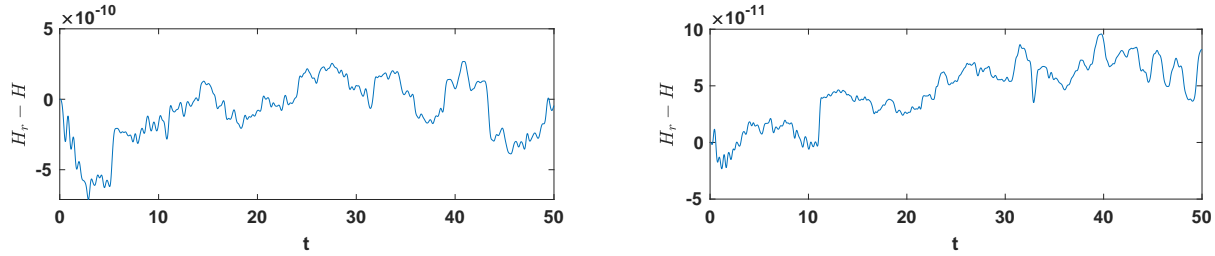


Figure 6: Time evolution of energy error $H_r \Delta x - H \Delta x$ in SP-DEIM-2: $r = 10$ (left) and $r = 20$ (right).

3.4 Summary of numerical experiments

We summarize the above test cases in Tables 1-2. The results are benchmarked by the full order solutions: the discrete Hamiltonian value is $H \Delta x = 1.258 \times 10^{-1}$ and the CPU time for the full order simulation is $t_{cpu} = 52.8$ seconds.

Table 1: Nonlinear wave equations: comparison of ROMs (r=10)

	G-ROM	SP-POD-1	SP-POD-2	SP-DEIM-1	SP-DEIM-2
\mathcal{E}_∞	3.291×10^{-2}	3.291×10^{-2}	3.711×10^{-2}	3.365×10^{-2}	3.490×10^{-2}
$H_r \Delta x - H \Delta x$	$\mathcal{O}(10^{-5})$	$\mathcal{O}(10^{-5})$	$\mathcal{O}(10^{-10})$	$\mathcal{O}(10^{-5})$	$\mathcal{O}(10^{-10})$
t_{cpu} (s)	0.755	0.601	0.630	0.140	0.143

Based on the results, we can draw the following conclusions: (i) the structure-preserving ROMs with basis from shifted snapshots (SP-POD-2 and SP-DEIM-2) are able to preserve the energy, which achieve better Hamiltonian approximations than other ROMs; (ii) using the SP-DEIM models reduces the CPU time of their SP-POD counterparts; The speedup factor could be larger if the nonlinear function is more complicated or the dimension of the full order model

Table 2: Nonlinear wave equations: comparison of ROMs (r=20)

	G-ROM	SP-POD-1	SP-POD-2	SP-DEIM-1	SP-DEIM-2
\mathcal{E}_∞	8.288×10^{-3}	8.298×10^{-3}	1.152×10^{-2}	8.473×10^{-3}	1.311×10^{-2}
$H_r \Delta x - H \Delta x$	$\mathcal{O}(10^{-7})$	$\mathcal{O}(10^{-7})$	$\mathcal{O}(10^{-11})$	$\mathcal{O}(10^{-7})$	$\mathcal{O}(10^{-11})$
t_{cpu} (s)	0.979	0.786	0.805	0.209	0.210

is bigger; (iii) using the SP-DEIM models achieves approximation errors close to their SP-POD counterparts; Such differences would be negligible when more DEIM basis and interpolation points are included; and (iv) overall, SP-DEIM-2 outperforms the other ROMs discussed in this paper in terms of discrete Hamiltonian approximation, the accuracy and efficiency of reduced order simulations.

4 Conclusions

Energy preserving schemes have been developed for simulating Hamiltonian PDEs, for which one significant property is to preserve the Hamiltonian function. When model reduction techniques such as the POD method is applied, the standard Galerkin projection would destroy this property, thus the discrete Hamiltonian is not well preserved. In [1], the structure-preserving POD have been developed that keeps the coefficient matrix skew symmetric in the ROMs, which achieves a constant Hamiltonian approximation. However, the computational complexity of the SP-POD ROMs is still high at the online stage. Therefore, a new structure-preserving DEIM has been introduced in this paper to improve the online efficiency while obtaining an accurate Hamiltonian approximation from the reduced order simulations. Numerical experiments demonstrate the efficacy of the proposed approach.

5 Acknowledgements

Z. Wang's research was partially supported by the National Science Foundation through grants DMS-1913073 and DMS-2012469, and by the US Department of Energy through grant SC0020270.

References

- [1] Yuezheng Gong, Qi Wang, and Zhu Wang. Structure-preserving galerkin pod reduced-order modeling of hamiltonian systems. *Computer Methods in Applied Mechanics and Engineering*, 315:780–798, 2017.
- [2] E. Hairer, C. Lubich, and G. Wanner. Geometric numerical integration: Structure preserving algorithms for ordinary differential equations. *Springer-Verlag, Berlin*, 2002.

- [3] K. Feng and M. Qin. Symplectic geometric algorithms for hamiltonian systems. *Heidelberg, Dordrecht, London, New-York: Springer*, 2010.
- [4] T.J. Bridges and S. Reich. Numerical methods for Hamiltonian PDEs. *J. Phys. A: Math. Gen.*, 39:5287–5320, 2006.
- [5] Y. Wang and J. Hong. Multi-symplectic algorithms for hamiltonian partial differential equations. *Commun. Appl. Math. Comput.*, 27:163–230, 2013.
- [6] O. Gonzalez. Time integration and discrete hamiltonian systems. *J. Nonlinear Sci.*, 6:449–467, 1996.
- [7] R.I. McLachlan, G.R.W. Quispel, and N. Robidoux. Geometric integration using discrete gradients. *Philos. Trans. Roy. Soc. London Ser. A: Math. Phys. Eng. Sci.*, 357:1021–1045, 1999.
- [8] G.R.W. Quispel and D.I. McLaren. A new class of energy-preserving numerical integration methods. *J. Phys. A: Math. Theor.*, 41:045206 (7pp), 2008.
- [9] E. Celledoni, V. Grimm, R.I. McLachlan, D.I. McLaren, D. O’Neale, B. Owren, and G.R.W. Quispel. Preserving energy resp. dissipation in numerical pdes using the “average vector field” method. *J. Comput. Phys.*, 231:6770–6789, 2012.
- [10] Y. Gong, J. Cai, and Y. Wang. Some new structure-preserving algorithms for general multi-symplectic formulations of Hamiltonian PDEs. *J. Comput. Phys.*, 279:80–102, 2014.
- [11] T. Bui-Thanh, K. Willcox, O. Ghattas, and B. van Bloemen Waanders. Goal-oriented, model-constrained optimization for reduction of large-scale systems. *Journal of Computational Physics*, 224(2):880–896, 2007.
- [12] K. Carlberg and C. Farhat. A low-cost, goal-oriented compact proper orthogonal decomposition basis for model reduction of static systems. *International Journal for Numerical Methods in Engineering*, 86(3):381–402, 2011.
- [13] S. Chaturantabut, D. C. Sorensen, and J. C. Steven. Nonlinear model reduction via discrete empirical interpolation. *SIAM Journal on Scientific Computing*, 32(5):2737–2764, 2010.
- [14] D. N. Daescu and I. M. Navon. A dual-weighted approach to order reduction in 4DVAR data assimilation. *Monthly Weather Review*, 136(3):1026–1041, 2008.
- [15] P. Holmes, J. L. Lumley, and G. Berkooz. *Turbulence, Coherent Structures, Dynamical Systems and Symmetry*. Cambridge University Press, Cambridge, UK, 1996.
- [16] A. Iollo, S. Lanteri, and J. A. Désidéri. Stability Properties of POD-Galerkin Approximations for the Compressible Navier–Stokes Equations. *Theoretical and Computational Fluid Dynamics*, 13(6):377–396, 2000.

- [17] K. Kunisch and S. Volkwein. Galerkin proper orthogonal decomposition methods for parabolic problems. *Numerische Mathematik*, 90(1):117–148, 2001.
- [18] S Sirisup and GE Karniadakis. A spectral viscosity method for correcting the long-term behavior of pod models. *Journal of Computational Physics*, 194(1):92–116, 2004.
- [19] Toni Lassila, Andrea Manzoni, Alfio Quarteroni, and Gianluigi Rozza. Model order reduction in fluid dynamics: challenges and perspectives. In *Reduced Order Methods for modeling and computational reduction*, pages 235–273. Springer, 2014.
- [20] Christopher Beattie and Serkan Gugercin. Structure-preserving model reduction for nonlinear port-hamiltonian systems. In *Decision and Control and European Control Conference (CDC-ECC), 2011 50th IEEE Conference on*, pages 6564–6569. IEEE, 2011.
- [21] Saifon Chaturantabut, Chris Beattie, and Serkan Gugercin. Structure-preserving model reduction for nonlinear port-hamiltonian systems. *SIAM Journal on Scientific Computing*, 38(5):B837–B865, 2016.
- [22] Liqian Peng and Kamran Mohseni. Symplectic model reduction of hamiltonian systems. *SIAM Journal on Scientific Computing*, 38(1):A1–A27, 2016.
- [23] Bülent Karasözen and Murat Uzunca. Energy preserving model order reduction of the nonlinear schrödinger equation. *Advances in Computational Mathematics*, 44(6):1769–1796, 2018.
- [24] Bülent Karasözen, Süleyman Yıldız, and Murat Uzunca. Structure preserving model order reduction of shallow water equations. *Mathematical Methods in the Applied Sciences*, 44(1):476–492, 2021.
- [25] S. Chaturantabut and D. C. Sorensen. A state space error estimate for POD-DEIM nonlinear model reduction. *SIAM Journal on Numerical Analysis*, 50:46, 2012.
- [26] Yuto Miyatake. Structure-preserving model reduction for dynamical systems with a first integral. *Japan Journal of Industrial and Applied Mathematics*, 36(3):1021–1037, 2019.
- [27] Babak Maboudi Afkham and Jan S Hesthaven. Structure preserving model reduction of parametric hamiltonian systems. *SIAM Journal on Scientific Computing*, 39(6):A2616–A2644, 2017.
- [28] Babak Maboudi Afkham and Jan S Hesthaven. Structure-preserving model-reduction of dissipative hamiltonian systems. *Journal of Scientific Computing*, 81(1):3–21, 2019.
- [29] Jan S Hesthaven, Cecilia Pagliantini, and Nicolò Ripamonti. Rank-adaptive structure-preserving reduced basis methods for hamiltonian systems. *arXiv preprint arXiv:2007.13153*, 2020.
- [30] Cecilia Pagliantini. Dynamical reduced basis methods for hamiltonian systems. *arXiv preprint arXiv:2008.07427*, 2020.

- [31] Kevin Carlberg, Ray Tuminaro, and Paul Boggs. Preserving lagrangian structure in nonlinear model reduction with application to structural dynamics. *SIAM Journal on Scientific Computing*, 37(2):B153–B184, 2015.
- [32] Charbel Farhat, Todd Chapman, and Philip Avery. Structure-preserving, stability, and accuracy properties of the energy-conserving sampling and weighting method for the hyper reduction of nonlinear finite element dynamic models. *International Journal for Numerical Methods in Engineering*, 102(5):1077–1110, 2015.
- [33] E. Hairer. Energy-preserving variant of collocation methods. *J. Numer. Anal. Ind. Appl. Math.*, 5:73–84, 2010.
- [34] D. Cohen and E. Hairer. Linear energy-preserving integrators for poisson systems. *BIT Numer. Math.*, 51:91–101, 2011.
- [35] M. Dahlby and B. Owren. A general framework for deriving integral preserving numerical methods for pdes. *SIAM J. Sci. Comput.*, 33:2318–2340, 2011.